

Probing a Non-Thermal Plasma Activated Heterogeneously Catalyzed Reaction Using in Situ DRIFTS-MS

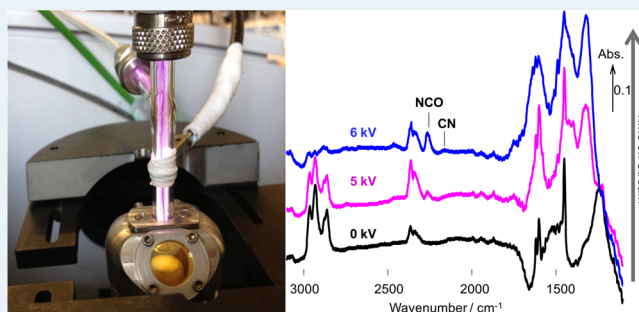
C. E. Stere,[†] W. Adress,[‡] R. Burch,[†] S. Chansai,[†] A. Goguet,[†] W. G. Graham,^{*,‡} and C. Hardacre^{*,†}

[†]Centre for the Theory and Application of Catalysis, CenTACat, School of Chemistry and Chemical Engineering and [‡]Centre for Plasma Physics, School of Mathematics and Physics, Queen's University Belfast, Belfast BT9 5AG, Northern Ireland, U.K.

Supporting Information

ABSTRACT: The current paper reports on a newly developed DRIFTS-MS system for the investigation of non-thermal plasma (NTP) assisted heterogeneously catalyzed reactions. Specifically, this methodology has been utilized to investigate the surface changes during the NTP-activated hydrocarbon selective catalytic reduction (HC-SCR) deNO_x reaction over a silver-based catalyst at ambient temperature using simulated diesel fuels (toluene and *n*-octane). The experimental setup and the methods used to investigate the plasma activation operating with helium as the carrier gas in order to examine low-temperature reactions are described. The technique has identified the importance, even at low temperatures, of isocyanate species in the HC-SCR deNO_x reaction as well as the critical role of water in the formation of N₂.

KEYWORDS: low-temperature hydrocarbon-selective catalytic reduction, Ag/Al₂O₃, non-thermal plasma, DRIFTS-MS, NO_x reduction, toluene, octane

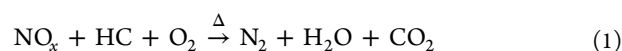


1. INTRODUCTION

Although a significant number of studies have examined the use of plasmas to activate heterogeneously catalyzed processes, few investigations^{1–3} have used in situ methods to understand the effect of the plasma on the catalytic reaction mechanism and thus provide a method to optimize both the catalyst as well as the plasma operating parameters. The present paper gives a detailed description of a diffuse reflectance infrared (DRIFTS) cell designed for the investigation of plasma assisted gas phase heterogeneously catalyzed reactions. This new methodology has been used to investigate the mechanism of the hydrocarbon assisted selective catalytic reduction (HC-SCR) deNO_x reaction over silver-based catalysts both under plasma activation and in the absence of plasma. The evolution of the gas phase reactant species and formation of reaction products was monitored simultaneously by DRIFTS and mass spectrometry (MS).

The properties observed for combined catalyst–plasma systems^{4–10} show some promise for selective NO_x reduction by hydrocarbons over Ag/Al₂O₃ catalysts, since the activation or partial oxidation of the hydrocarbons is a controlling step in the formation of N₂ as a product.

The conventional thermal activation reaction is given by



The enhancement in hydrocarbon activation by plasma processes is generally attributed to the direct interaction of the radicals, electrons, and UV photons created by the plasma with the catalyst and molecules adsorbed on its surface.^{11–13} This

enhancement has been reported recently by our group to result in a significant increase in the activity of silver-based catalysts during the HC-SCR deNO_x reaction.⁴ Therein, conversions of NO_x to N₂ of ~40% and 50% were observed using toluene and *n*-octane as the reductants, respectively, under ambient-temperature conditions. This activity was found to be strongly correlated with the voltage of the plasma applied. In the case of toluene-SCR, increased conversion of both toluene and NO_x was found with increasing applied potential from 5 to 7 kV. In contrast, for *n*-octane-SCR, although *n*-octane conversion was found to increase in a similar manner, the NO_x conversion was found to go through a maximum that was attributed to the switch from partial oxidation of the hydrocarbon, which results in NO_x reduction activity, to complete conversion of the hydrocarbon, which results in a decrease in the reduction of NO_x. Importantly, this low-temperature activity may be compared with the reaction temperatures of above 400 °C which are typically required for equivalent conversions for the thermally activated process.^{14–17} It should be noted that the plasma activated catalyst leads to essentially the same selectivity as for the thermally activated process with high N₂ selectivity and only small amounts of N₂O; however, in particular for the toluene-SCR deNO_x reaction, the plasma activated system has been found to deactivate significantly more slowly in comparison to that for thermal activation. In addition, by measurement of the

Received: December 2, 2014

Revised: December 21, 2014

Published: December 23, 2014

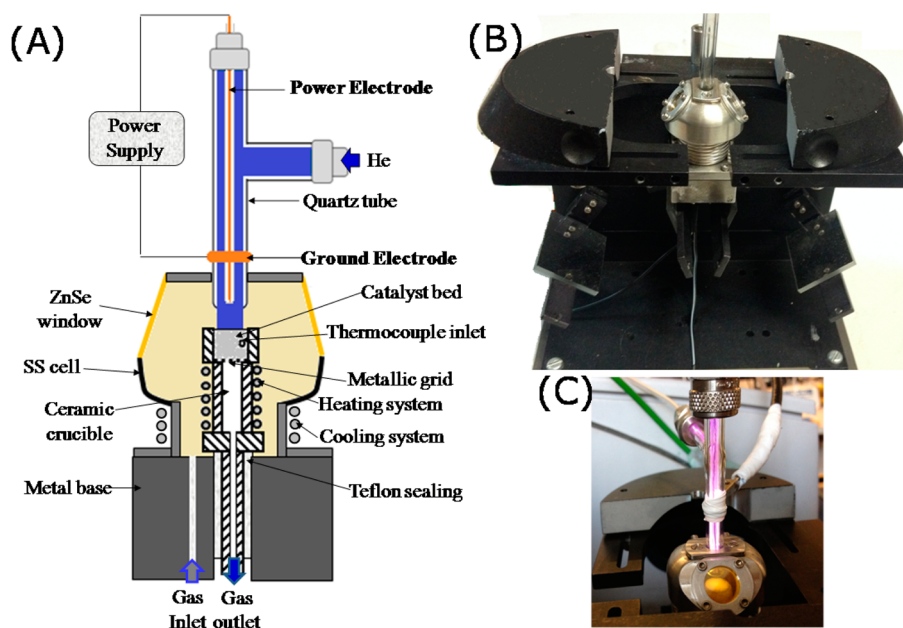


Figure 1. DRIFTS-MS setup: (A) schematic sketch of the modified dome for the NTP-DRIFTS-MS measurements; photograph of the (B) setup and (C) the metallic dome with plasma on.

power consumption of the oven in comparison with the power supply used for the plasma generation, a reduction in the energy used of 45% was found even for the unoptimized system.

The current paper reports on a newly developed DRIFTS-MS system utilized to investigate the surface changes during the non-thermal plasma (NTP) activated HC-SCR deNO_x reaction over a silver-based catalyst using simulated diesel fuels (toluene and *n*-octane) with helium as discharge medium. The use of He as balance gas enabled the study of HC-assisted NO_x removal at low temperature (25 °C). The experimental setup and the methods used to investigate the plasma activation are described. The technique has identified the importance of isocyanate species in the HC-SCR reaction as well as the critical role of water in the formation of N₂.

2. EXPERIMENTAL SECTION

The catalyst used in this study was 2.0% Ag/Al₂O₃ provided by Johnson Matthey, and it was prepared by impregnation of an γ -Al₂O₃ support (LaRoche Industries Inc.) as described elsewhere.⁴

The experimental setup consisted of a plasma-IR-MS coupled system developed in house and described in detail in section 3.1. In situ DRIFTS measurements were performed using a Bruker Vertex 70 FTIR spectrometer equipped with a liquid N₂ cooled detector.

The gases for the reaction mixture were supplied by BOC, and each was individually controlled by an Aera FC-7700C mass flow controller. The total flow rate and space velocity of the gas mixture were 100 cm³ min⁻¹ and 165600 cm³ g⁻¹ h⁻¹, respectively. The concentrations of the reactants used were 720 ppm of NO, 4.3% of O₂, 540 ppm of *n*-C₈H₁₈ or 620 ppm of toluene equivalent of 4340 ppm as C₁, 4.0% H₂O (when added), 0.3% Kr, and He balance. A fixed amount of the balance gas (50 cm³ min⁻¹ He) was passed from the top of the IR cell, through a 4 mm i.d. quartz tube for plasma generation (Figure 1), and the remainder from the bottom of the cell, together with the other gases.¹⁸ *n*-Octane, toluene, and water vapor were introduced by passing He as a carrier gas through separate custom-made saturators. The hydrocarbon saturator was

placed in an ice/water bath, and the H₂O saturator temperature was controlled using a Grant GD120 thermostatic bath.

In order to monitor the changes of gas phase species, the outlet of the DRIFTS cell was connected to a Hidden Analytical HPR20 mass spectrometer via a heated capillary. The following mass to charge (*m/z*) ratios were monitored by the MS as a function of time: 18 (H₂O), 28 (CO, N₂), 30 (NO), 31 (O₂), 44 (CO₂), 46 (NO₂), 57 (*n*-C₈H₁₈) or 92 (C₇H₈), and 82 (Kr). Due to the high signal for *m/z* 32, *m/z* 31 was used to monitor the O₂ signal. Quantification was carried out with reference to the Kr signal and subtraction of the blank reactor profile. All of the reactions were carried out at ambient temperature.

The in situ DRIFTS spectra were recorded every 10 s with a resolution of 4 cm⁻¹ and were analyzed with the OPUS software. The IR data are reported as log 1/*R* ("absorbance"), with $R = I/I_0$, where *R* is the sample reflectance, *I* the intensity measured under reaction conditions, and *I*₀ the intensity measured on the sample under a flow of helium (see ref 19 for the full details). The *I*₀ background spectrum was recorded at room temperature, immediately prior to the introduction of the reactant mixture.²⁰

The atmospheric pressure non-thermal plasma was generated using an ac power supply (Model PVM500). A high-voltage probe (Tektronix, P6015) and the voltage drop across a 50 Ω resistance in the return line to the grounded electrode were used to determine the voltage–current characteristics of the system. The powered electrode was driven at ~20 kHz with peak applied voltages from 4 to 7.5 kV. A representative example of the time-resolved voltage and current measurements is given in Figure S1 in the Supporting Information.

The gas temperature during the plasma-SCR experiments was determined from the rotational temperature *T*_{rot} of the nitrogen molecules determined spectroscopically from the $\nu = 0$ to 2 rotational band of the N₂ (C³Π_u⁺) to (B³Π_g⁺) second positive system²¹ (Figure S2 in the Supporting Information) recorded with an Ocean Optics imaging spectrometer. A *K*-type grounded thermocouple was placed in the center of the catalyst bed for temperature measurements in the absence of plasma.

3. RESULTS

3.1. Technique Development: Plasma-Coupled DRIFTS-MS Experiments. The experiments were designed to obtain more insight into how the helium–atmospheric pressure non-thermal plasma can enhance the SCR activity of the silver catalyst at ambient temperature. Figure 1 shows a schematic and photographs of the NTP-DRIFTS-MS setup. Importantly, the dome was designed to allow sufficient space for the plasma stream to be placed within the cell and interact with the catalyst bed directly while also allowing a line of sight for the infrared signal to pass through the windows and reflect on and off the catalyst bed. Therefore, it is important to note that the IR beam was focused on the center of the catalyst bed at the same point as where the plasma discharge was in direct contact with the solid surface of the catalyst to ensure that the DRIFTS was representative of the plasma activated surface. All of the spectra taken when the NTP was on were obtained with the IR beam and NTP in contact with the same position on the catalyst surface to ensure that the signals are representative of the plasma activated system.

The catalyst was supported by an inert metallic mesh in a ceramic crucible within a high-temperature DRIFTS cell that was developed in house. Teflon tape was used to seal the metallic base plate to the reactor crucible. The cell was connected to the feed gas cylinders through low-volume stainless steel tubing, and the reaction flow was fed through the reactor bed such that the upper layer of catalyst was at the front of the reaction zone and probed by the infrared radiation.^{19,20} This enabled the front face of the catalyst bed and the NTP plume to be in direct contact. It had been shown previously⁴ that this is a critical requirement to ensure high activity of the plasma–catalyst hybrid system.

The plasma conduit was designed to ensure that the electrodes generating the plasma would not arc to the metal body of the DRIFTS cell. Therefore, as shown in Figure 1, the ring electrode dielectric barrier plasma design used in ref 4 was adapted by replacing the power ring electrode with a 0.7 mm diameter tungsten wire encompassed in a sealed 1.1 mm thick quartz tube. The capillary was vertically suspended in a “T”-shaped quartz tube (o.d. 6 mm, i.d. 4 mm) that was in turn attached to the metallic dome, as shown in Figure 1. While atmospheric pressure plasma jet devices using a bare pin or needle as a driving electrode have been previously reported,^{22–24} to the best of our knowledge, there have been no previous reports on the use of a dielectric enclosed electrode such as that described in this work.

The tip of the dielectric capillary was positioned 1.6 mm from the end of the “T”-shaped tube and 10 mm from the 2 mm wide, grounded circular copper ring, leaving a clear pathway to allow the infrared signal to pass through the windows and reflect off the catalyst bed. Helium was flowed from the side arm of the “T”-shaped discharge tube at a flow rate of 50 cm³ min⁻¹ in order to generate a NTP directly onto the catalyst bed.

3.2. Effect of the Applied Voltage on the SCR Activity. Figure 2 shows the in situ DRIFTS spectra of surface species adsorbed on Ag/Al₂O₃ catalyst during the *n*-octane-SCR (A) and toluene-SCR (B) of NO_x for a dry feed (720 ppm of NO, 4340 ppm of C₈H₁₈ as C₁, 4% O₂, and He balance) in the presence of the plasma at ambient temperature.

For the *n*-octane-SCR no NO_x reduction was observed at 25 °C in the absence of the NTP. In this case, a band at 1243 cm⁻¹, which is assigned to nitrites,^{15,16,25–31} was observed together with IR bands between 3100 and 2800 cm⁻¹, which are attributed

to adsorbed and gas phase *n*-octane.^{15,16,29–31} However, significant changes were observed in the DRIFTS spectra when plasma was generated. On application of a 5 kV voltage to the system for 1 min, the adsorbed nitrites at 1243 cm⁻¹ disappeared and a band at 1312 cm⁻¹, assigned to nitrate species,^{15,16,25–35} developed, as well as the formation of an acetate-based feature at 1450 cm⁻¹^{15,25,27,30,32,33} and a carboxylate band at 1595 cm⁻¹.^{15,25,27,30,32,33} More importantly, a small band associated with adsorbed –NCO at 2260 cm⁻¹ was also observed.^{15,16,25–36} After 10 min of plasma activation at 5 kV, further increases in the acetate, nitrate, carboxylate, and isocyanate bands were observed and it is clearly seen that the *n*-octane bands decreased, indicating conversion of the hydrocarbon.

In agreement with our previous study,⁴ the SCR activity was improved by increasing the applied voltage, therefore enhancing the number of long-lived species (e.g. ozone) and short-lived species (He*, N₂, N₂⁺, O₂), as observed in the optical emission spectroscopy measurements in N₂ and broad-band regions.^{11–13,37} Thus, at 6 kV almost complete conversion of the hydrocarbon was observed (shown by the disappearance of the *n*-octane bands) and further increases in the bands assigned to adsorbed isocyanate, nitrate, carboxylate, formate, and acetate species. In addition, a very small band associated with cyanide at 2165 cm⁻¹ was observed. In comparison with the thermal activation of *n*-octane,^{14–17,38} it was observed that, with the plasma, significantly less –CN is being formed and then only with increasing time on stream. The presence of isocyanate, in particular given that this is the only species observed (i.e. no cyanide is found) under certain conditions which are observed to promote deNO_x activity, indicates that the mechanism for the plasma activated *n*-octane-SCR reaction is likely to be the same as that found under thermally activated conditions. In this case, these results support the proposal that isocyanate is the key intermediate for the deNO_x reaction and not cyanide.

In general, similar behavior was also observed for the toluene-SCR reaction. In the region 1200–1800 cm⁻¹ removal of nitrites and formation of nitrate, formate, acetate, carbonate, and carboxylate species in the presence of NTP was observed. However, an important difference between the aliphatic and aromatic hydrocarbons tested was found between 2100 and 2300 cm⁻¹. In the presence of toluene, –NCO formation was not detected under any of the conditions tested; the only intermediate formed was –CN, and this band increased with increasing voltage. In order to clarify the role of –CN in the toluene-SCR reaction, the reaction was studied in the presence of water and on switching the plasma on and off.

3.3. Influence of Water on the SCR Activity. Water is known to be critical in the formation of N₂ in HC-SCR reactions over silver-based catalysts,^{14,17,29,34–36,38–41} and thus the influence of water in the presence of the NTP was examined. Figure 3A presents the DRIFTS spectra during the toluene-SCR of NO_x with 4% H₂O in the feed, over the Ag/Al₂O₃ catalyst. On application of the NTP, cyanide bands at 2165 cm⁻¹ were observed and they increased with applied voltage. However, no significant adsorbed –NCO was observed. The experiments with NTP would indicate that, in the presence of water, the formation rate of the cyanide species is fast in comparison with their further reaction; hence, they build up on the surface of the catalyst, most probably on the alumina support.^{32–34,38,39} There are, however, various debates on the role of the cyanides in the conventional thermally

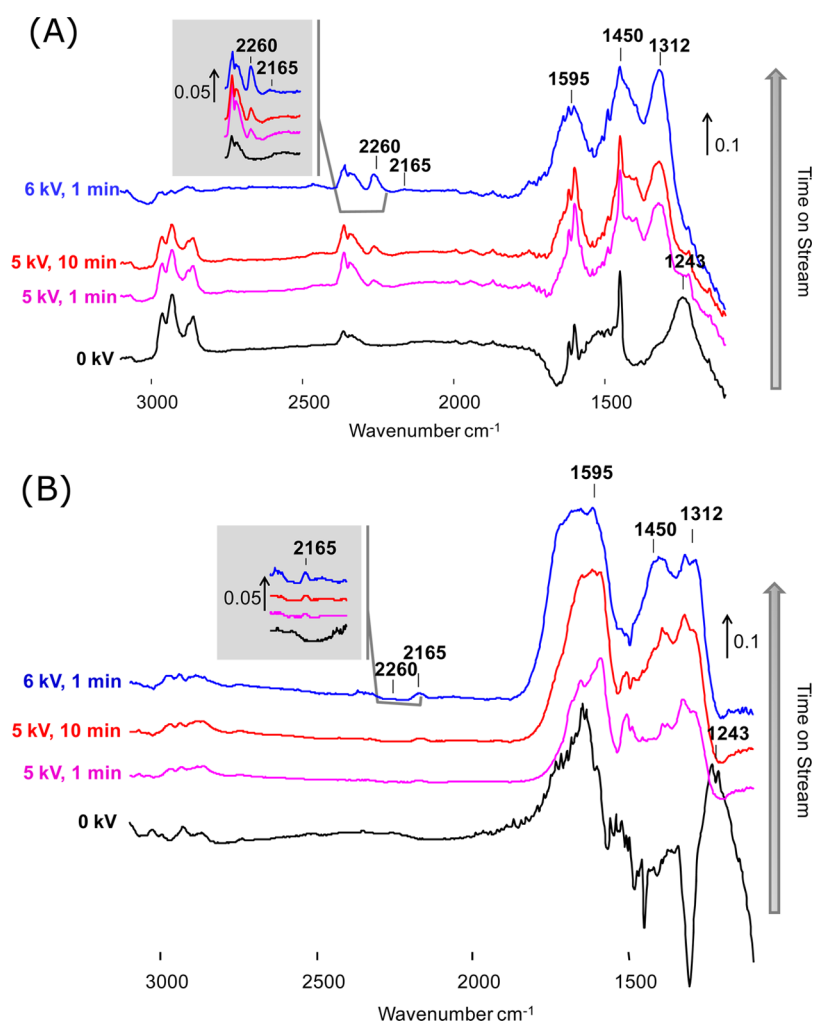
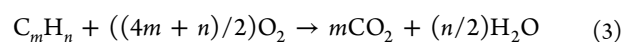
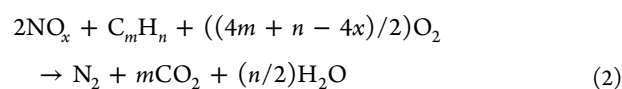


Figure 2. Changes in surface species observed during the (A) *n*-octane-SCR and (B) toluene-SCR of NO_x over 2 wt % Ag/Al₂O₃ with and without plasma. Feed composition: 720 ppm of NO, 540 ppm of *n*-C₈H₁₈ or 620 ppm of C₈H₁₈ equivalent of 4340 ppm as C₁, 4.3% of O₂, and He balance. The total flow rate was 100 cm³ min⁻¹.

activated HC-SCR of NO_x over silver catalysts. A number of studies^{15,34,35} have pointed out the importance of transforming cyanide into isocyanate, through isomerization and oxidation reactions. Tamm et al.²⁹ proposed two distinct routes for the reduction of NO_x: one through cyanide and a different one through isocyanate species. Therein, it was argued that the formation of -NCO species is preceded by the reaction of surface nitrates with surface C-containing compounds, possibly implying an organo-nitro compound, while the precursor of the cyanide is an oxime, formed by the tautomerization of organo-nitroso compounds, formed by the interaction between C-containing compounds and short-lived N-containing surface species or gas-phase NO_x. It has also been reported that water hydrolyzes the isocyanates to form NH₃ on the Ag sites^{14,17,29,34–36,39} during the SCR reaction; thus, if the rate of hydrolysis is high, the presence of -NCO species might not be observed,^{29,42} even if they are formed. It is worth mentioning that the gas phase NH₃ formation or release could not be observed due to the presence of 4% H₂O and the overlap between fragments of water and ammonia. Therefore, the formation of ammonia cannot be ruled out under these conditions.

The overall conversion of the NO_x and hydrocarbon in the presence of water was calculated from the MS data and is presented in Figure 3, together with the MS signals attributed

to H₂ (*m/z* 2) and CO₂ formation (*m/z* 44). At voltages lower than 6 kV, the NTP did not have a dramatic impact on the SCR activity, with <10% toluene conversion and a maximum of 18% reduction of NO_x observed. However, the conversion increased by applying a higher voltage to the system. Thus, it was found that, with 7.5 kV, about 30% of the gas phase toluene was consumed and the NO_x conversion reached ~45%. It is important to note that the reactor configuration can play a very important role in the type of plasma that is generated and subsequently in the activity of the catalyst while the discharge is on. We have reported previously that the applied voltage and frequency would influence not only the conversion of NO_x and hydrocarbon but also the selectivity of the hydrocarbon toward SCR of NO_x in comparison with complete oxidation.⁴ The results herein indicate that, with the current reactor configuration, the toluene showed a high selectivity toward the SCR of NO_x (eq 2) rather than complete oxidation (eq 3), when NTP was applied to the system.



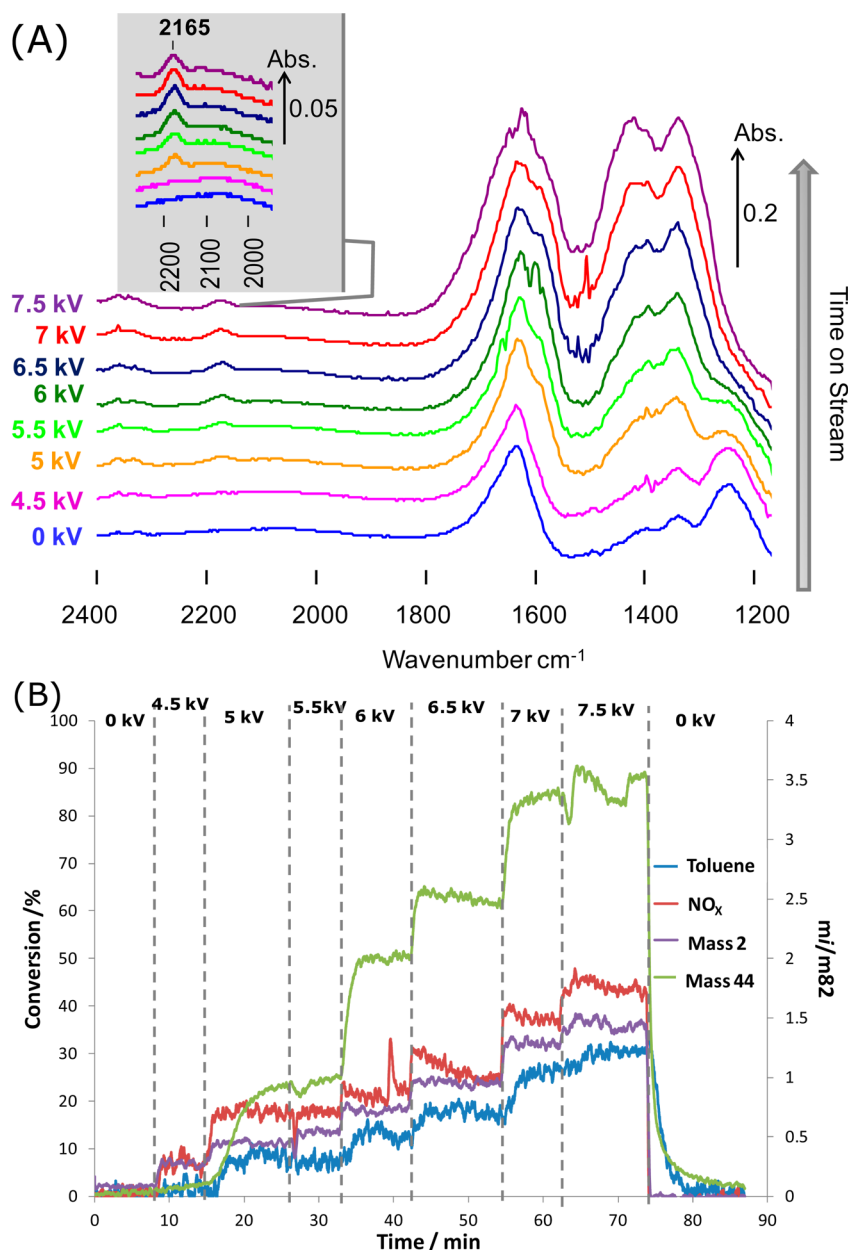
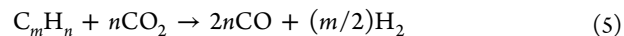
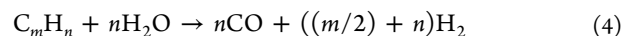


Figure 3. Effect of applied voltage on the NO_x and hydrocarbon conversion during the toluene-SCR of NO_x reaction over 2 wt % $\text{Ag}/\text{Al}_2\text{O}_3$: (A) DRIFTS results; (B) MS results. Feed composition: 720 ppm of NO , 620 ppm of C_8H_{18} equivalent of 4340 ppm as C_1 , 4.3% of O_2 , 4% of H_2O , and He balance. The total flow rate was $100 \text{ cm}^3 \text{ min}^{-1}$.

On switching on the plasma initially, there was a delay in the response for the CO_2 production and toluene conversion. The latter is believed to be due to the fact that the surface will be saturated with toluene and, when the plasma is switched on, the catalyst surface will need to be cleaned to free up sites before further toluene activation is possible. This is not seen for the NO_x , for example, as the storage capacity for the hydrocarbon will be much higher than that for the NO_x . The delay in the CO_2 may be associated with the fact that, in the present arrangement, the plasma does not penetrate through the entire catalyst bed and thus the CO_2 formed at the front end of the catalyst bed will readsorb further down the bed where there is no reaction. This slows down the exit of the CO_2 and thus reduces the response time of the CO_2 signal to the initial change in the plasma condition.

The signal for mass 2 (assigned to hydrogen) was found to increase with the plasma voltage, indicating that some reforming reactions also occur under these conditions (eqs 4 and 5).



Lee et al.⁴³ also reported that onboard plasma reforming can be an important strategy for effective HC-SCR over $\text{Ag}/\text{Al}_2\text{O}_3$ catalysts. They found that hydrogen produced through plasma reforming only promotes partial oxidation of hydrocarbon to yield surface intermediates that significantly facilitate SCR, which is consistent with the results shown herein. However, it should be noted that hydrogen is known to promote the SCR

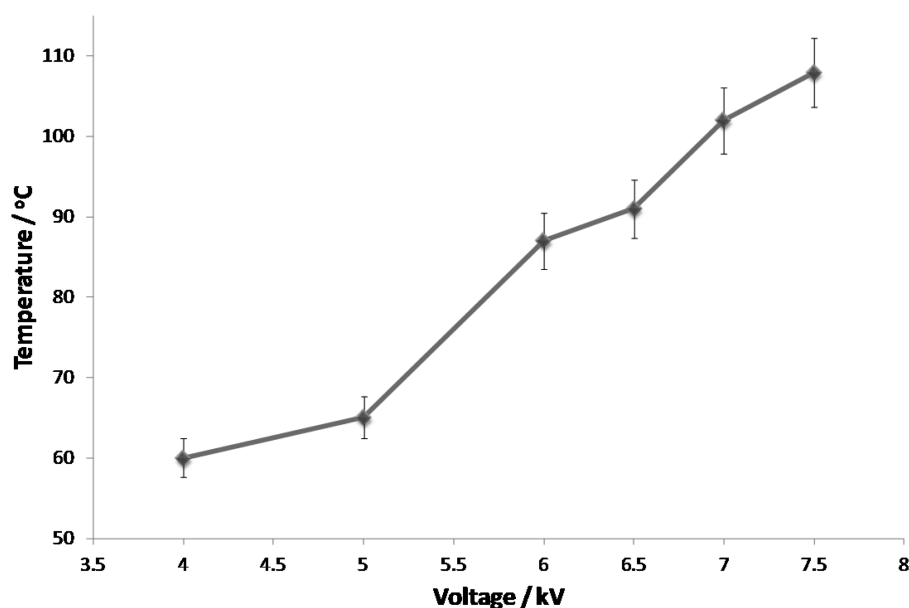


Figure 4. Rotational gas temperature of the toluene-SCR reaction over $\text{Ag}/\text{Al}_2\text{O}_3$ catalyst, as a function of the plasma applied voltage. The measurement was conducted at 20 kHz, and the total flow rate was $100 \text{ cm}^3 \text{ min}^{-1}$.

activity of the silver catalyst at temperatures higher than $150 \text{ }^\circ\text{C}$. From the rotational gas temperature measurements performed, we have observed that for all conditions investigated the temperature was never higher than $110 \text{ }^\circ\text{C}$. Figure 4 shows the measured rotational gas temperatures, which we infer is also the gas temperature,⁴⁴ for different electrode voltages, all measured at 2.85 cm above the catalyst bed during a toluene-SCR reaction. It can be seen that the temperature increased from $60 \text{ }^\circ\text{C}$ at 4.5 kV to $108 \text{ }^\circ\text{C}$ at 7.5 kV. This confirms that the activity of the catalyst for the NO_x SCR is not likely to have a significant contribution from thermal activation of the catalyst by gas heating but rather the plasma generated species that can interact with the silver catalyst.

3.4. Plasma On–Off Cycles. Figure 5A shows the effect of five plasma on–off cycles at regular intervals of 10 min using an applied voltage of 7 kV and a feed composition of 720 ppm of NO , 4.3% of O_2 , 620 ppm of toluene, 4.0% of H_2O , 0.3% of Kr, and He balance. A small deactivation of the catalyst was observed with cycle time, with the NO_x conversion dropping from 37% in the first cycle to $\sim 30\%$ in the fifth cycle. A similar drop is observed in the CO_2 MS signal, while the conversion of toluene and hydrogen was constant with cycling, indicating that the catalyst is not deactivating with respect to the reforming/partial oxidation processes. As expected on extinguishing the plasma, the conversion of NO_x and the formation of H_2 and CO_2 decrease, sharply mimicking the behavior found when the plasma is applied. While on the first cycle the toluene conversion sharply rises when the plasma is switched on, when the plasma is extinguished, the toluene conversion drops slowly and on all subsequent cycles there is a slow increase in the conversion on application and a slow decrease in conversion on removal of the plasma. In the absence of the plasma, partial oxidation of the toluene occurs, leaving behind residual surface hydrocarbon; this results in the slow decrease in toluene conversion as the surface is still active due to the presence of adsorbed $\text{C}_x\text{N}_y\text{O}_z$ species. However, full conversion to CO_2 is not possible. On the application of the plasma, the surface gradually is cleaned from these species, forming CO_2 ,

converting NO_x and gradually freeing up sites for gas phase toluene to react, leading to the initial lag in conversion.

A comparison of the DRIFT spectra during this cycling (Figure 5B) shows that, in the absence and presence of the plasma in the first cycle, the intensity of the cyanide band does not change significantly. Gradually, the $-\text{CN}$ band does decrease with cycle number, as shown by the bands from the third cycle, which is consistent with the small deactivation of the catalyst observed from the conversion data.

4. DISCUSSION

Hydrocarbon activation is widely accepted as a key step in the mechanism for HC-SCR of NO_x and it has been suggested by many studies that the isocyanates are the key intermediates involved in the HC-SCR reaction over $\text{Ag}/\text{Al}_2\text{O}_3$ catalysts to form N_2 .^{14,17,29,32,34–36,38–41} Interestingly, in the thermally activated reactions, for example with *n*-octane as the hydrocarbon, both isocyanates (2260 cm^{-1}) and cyanides (2165 cm^{-1}) were observed. However, while the isocyanate species have been shown to be very active in the SCR reaction under these conditions and a key intermediate in the NO_x removal mechanism; in contrast, the cyanide species are reported to be strongly adsorbed, resulting in inhibition of active Ag sites.^{32–34,38,39}

In the case of the hybrid plasma–catalyst system reported herein, in the absence of water, the formation of isocyanates was only detected with *n*-octane and it is believed that for this reductant the mechanism is similar to that accepted during thermal activation at higher temperatures. Toluene has not been studied using *in situ* DRIFTS in conventional thermal experiments, due to the high temperatures required for the hydrocarbon activation (above the temperature limit of the DRIFTS equipment) and the rapid deactivation of the catalyst when using toluene as a reductant. In the case of the plasma experiments at much lower temperatures, cyanide was the only species found and no isocyanate was detected. Due to the ease of hydrolysis of the $-\text{NCO}$ species to form ammonia, the presence or absence of the isocyanate features, even when water is not present, does not rule out their role in the HC-SCR

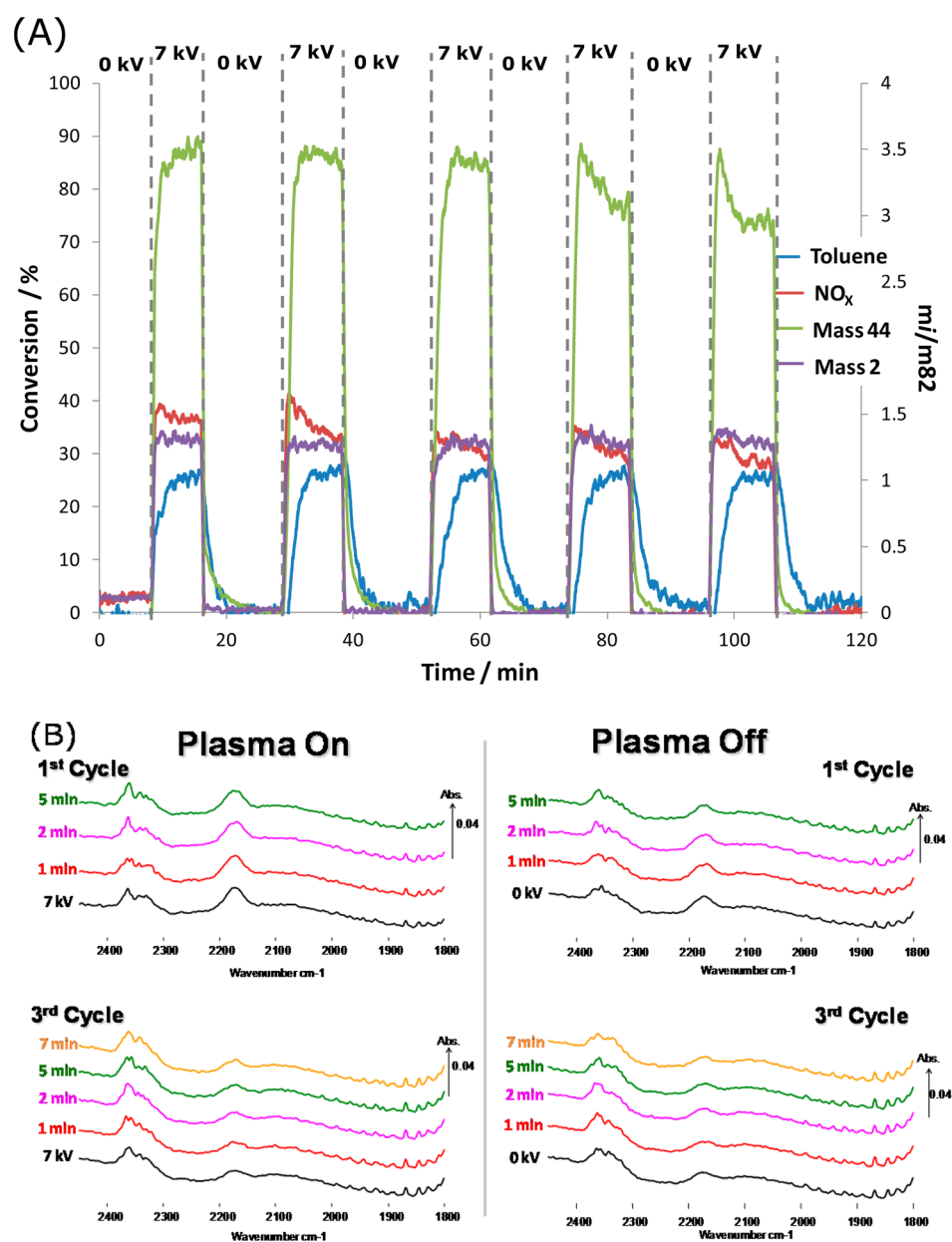


Figure 5. Plasma on–off switches during the toluene-SCR of NO_x over 2 wt % $\text{Ag}/\text{Al}_2\text{O}_3$: (A) MS results; (B) DRIFTS results. Feed composition: 720 ppm of NO , 620 ppm of C_8H_{18} equivalent of 4340 ppm as C_1 , 4.3% of O_2 , 4% of H_2O , and He balance. The total flow rate was $100 \text{ cm}^3 \text{ min}^{-1}$, and the applied voltage was 7 kV.

mechanism, as their surface concentration is determined by the rate of formation in comparison with their rate of hydrolysis.

In the case of *n*-octane, the hydrocarbon is much more easily oxidized, increasing the rate of formation of isocyanate species on the surface. These will be hydrolyzed to a small extent by the water formed from the oxidation of the hydrocarbon, and as this rate is low due to the low concentration of hydrocarbon-derived water formed, as opposed to when water is added to the feed, the isocyanate is observed under “dry” conditions. From the mechanism proposed by Meunier et al.²⁷ (Figure S3 in the Supporting Information), the $-\text{NCO}$ species can be formed directly via R-NO_2 compounds as well as from the conversion of cyanide. In contrast, cyanide is only formed via the R-ONO route. Therefore, the DRIFTS spectra from the plasma-activated reaction may indicate that, for the *n*-octane reaction, the pathway favored is via R-NO_2 rather

than R-ONO . This is due to the fact that only very small surface concentrations of cyanide, despite their high stability, are observed in comparison with isocyanate for plasma activation, whereas almost equal amounts are found for thermally activated catalyst.^{14–17,38}

In comparison with the *n*-octane oxidation, the toluene oxidation is much less facile, decreasing the rate of formation of isocyanate. In this case, hydrolysis will still occur due to the water formed during oxidation and the overall balance of low surface concentration and the associated removal by hydrolysis may explain why very little isocyanate was detected in the DRIFTS spectra. For the toluene-SCR reaction, it is possible that both the R-ONO and R-NO_2 based routes, or just the R-ONO route, may be occurring, due to the detection of $-\text{CN}$ but not $-\text{NCO}$.

Importantly, the $-\text{CN}$ species observed in the DRIFTS experiments are probably just an indicator that the $-\text{CN}$ species

forms on the active site before being transported to the support as the bands do not change significantly on the switching of the plasma on and off. The small decrease in the $-\text{CN}$ bands with cycling of the plasma is consistent with the deactivation of the catalyst possibly due to the strong adsorption of carbeneous materials from toluene at room temperature. The fact that the bands decrease as the conversion decreases indicates that there are some reactive $-\text{CN}$ species within the band observed, albeit probably not the most active intermediate species.

In terms of the role that the NTP plays in the formation of $-\text{CN}/-\text{NCO}$ species, it may activate the NO and hydrocarbon to form some surface species. However, a critical role of the NTP in the reaction is also to keep the surface clean, since deactivation of the SCR reaction is not as prevalent in the NTP activated system as in the thermally activated process. The dominant interactions of plasma assisted NO_x reduction can be attributed to O , O_3 , OH , HO_2 , and H_2O , as well as UV photons, which are the plasma reactive species. Thus, one could attribute the role of cleaning the catalyst surface to the ozone from the plasma activated gas feed³⁷ by preserving a certain population of OH species.

5. CONCLUSIONS

The results presented herein provide further evidence of the role of NTP in promoting the performance of the Ag catalyst at low reaction temperature. For the first time, a combined DRIFTS hybrid plasma system has been reported in order to probe the reaction mechanism during the reaction. From the DRIFTS data, it is thought that the mechanism for the *n*-octane-SCR in the presence of plasma is similar to that found for the reaction during thermal activation, with isocyanate being the active intermediate. The plasma studies provide further evidence of this hypothesis, as the selectivity toward cyanide in comparison with isocyanate is significantly lower than that reported for the thermal systems. This may also indicate that the major route in the case of *n*-octane is via the R- NO_2 species on reaction of the NO_x with the hydrocarbon. In contrast, the reduction of NO_x with toluene may follow a different pathway, since no isocyanate species were observed in the absence of water. However, it is also possible that the water converts isocyanate very rapidly to ammonia, for example, in the case of the toluene-SCR. In this case, the route via R-ONO may be important, leading to the formation of cyanide species. During the formation of N_2 , the cyanide could be converted to isocyanate, which is rapidly hydrolyzed to ammonia that then reacts with NO to give N_2 .

■ ASSOCIATED CONTENT

Supporting Information

The following file is available free of charge on the ACS Publications website at DOI: 10.1021/cs5019265.

Typical current–voltage sinusoidal waveforms, experimental emission spectra during the HC-SCR reaction, and schematics of the HC-SCR reaction ([PDF](#))

■ AUTHOR INFORMATION

Corresponding Authors

*E-mail for W.G.G.: b.graham@qub.ac.uk.

*E-mail for C.H.: c.hardacre@qub.ac.uk.

Notes

The authors declare no competing financial interest.

■ ACKNOWLEDGMENTS

This work was carried out as part of the “4CU” program grant (EP/K001329/1), aimed at sustainable conversion of carbon dioxide into fuels, led by the University of Sheffield and carried out in collaboration with the University of Manchester, Queen’s University Belfast, and University College London, and the CASTech project (EP/G02152X/1). W.A. acknowledges the support of the Iraqi Ministry of Higher Education and Scientific Research.

■ REFERENCES

- (1) Wu, J.; Xia, Q.; Wang, H.; Li, Z. *Appl. Catal., B* **2014**, *156–157*, 265–272.
- (2) Hueso, J. L.; Cotrino, J.; Caballero, A.; Espinós, J. P.; González-Elipe, A. R. *J. Catal.* **2007**, *247*, 288–297.
- (3) Li, J.; Goh, W. H.; Yang, X.; Yang, R. T. *Appl. Catal., B* **2009**, *90*, 360–367.
- (4) Stere, C. E.; Adress, W.; Burch, R.; Chansai, S.; Goguet, A.; Graham, W. G.; De Rosa, F.; Palma, V.; Hardacre, C. *ACS Catal.* **2014**, *4*, 666–673.
- (5) Li, J.; Ke, R.; Li, W.; Hao, J. *Catal. Today* **2007**, *126*, 272–278.
- (6) Than Quoc An, H.; Pam Huu, T.; Le Van, T.; Cormier, J. M.; Khacel, A. *Catal. Today* **2011**, *176*, 474–477.
- (7) Cho, B. K.; Lee, J.-H.; Crellin, C. C.; Olson, K. L.; Hilden, D. L.; Kim, M. K.; Kim, P. S.; Heo, I.; Oh, S. H.; Nam, I.-S. *Catal. Today* **2012**, *191*, 20–29.
- (8) Harling, A. M.; Demidyuk, V.; Fischer, S. J.; Whitehead, J. C. *Appl. Catal., B* **2008**, *82*, 180–189.
- (9) Wang, H. *Chem. Commun.* **2013**, *49*, 9353–9355.
- (10) Magureanu, M.; Piroi, D.; Mandache, N. B.; Părvulescu, V. I.; Părvulescu, V.; Cojocaru, B.; Cadigan, C.; Richards, R.; Daly, H.; Hardacre, C. *Appl. Catal., B* **2011**, *104*, 84–90.
- (11) Okubo, M.; Tanioka, A.; Kuroki, T.; Yamamoto, T. *IEEE T. Ind. Appl.* **2002**, *38*, 1196–1203.
- (12) Kim, H. H.; Ogata, A.; Futamura, S. *Appl. Catal., B* **2008**, *79*, 356–367.
- (13) Yu, Q. Q.; Wang, H.; Liu, T.; Xiao, L. P.; Jiang, X. Y.; Zheng, X. M. *Environ. Sci. Technol.* **2013**, *46*, 2337–2344.
- (14) Shimizu, K.; Satsuma, A. *Phys. Chem. Chem. Phys.* **2006**, *8*, 2677–2695.
- (15) Wichterlová, B.; Sazama, P.; Breen, J. P.; Burch, R.; Hill, C. J.; Čapek, L.; Sobalík, Z. *J. Catal.* **2005**, *235*, 195–200.
- (16) Sazama, P.; Čapek, L.; Drobná, H.; Sobalík, Z.; Dědeček, J.; Arve, K.; Wichterlová, B. *J. Catal.* **2005**, *232*, 302–317.
- (17) Ralphs, K.; D’Agostino, C.; Burch, R.; Chansai, S.; Gladden, L. F.; Hardacre, C.; James, S. L.; Mitchell, J.; Taylor, S. F. R. *Catal. Sci. Technol.* **2014**, *4*, 531–539.
- (18) Meunier, F. C.; Goguet, A.; Shekhtman, S.; Rooney, D.; Daly, H. *Appl. Catal. A* **2008**, *340*, 196–202.
- (19) Meunier, F. C.; Reid, D.; Goguet, A.; Shekhtman, S.; Hardacre, C.; Burch, R.; Deng, W.; Flytzani-Stephanopoulos, M. *J. Catal.* **2007**, *247*, 277–287.
- (20) Piccolo, L.; Daly, H.; Valcarcel, A.; Meunier, F. C. *Appl. Catal., B* **2009**, *86*, 190–195.
- (21) Twomey, B.; Nindrayog, A.; Niemi, K.; Graham, W. G.; Dowling, D. P. *Plasma Chem. Plasma Process* **2011**, *31*, 139–156.
- (22) Li, X.; Jia, P.; Yuan, N.; Fang, T.; Wang, L.; Li, X. *Physics of Plasmas; Physics of Plasmas* **2011**, *18*, 043505–043508.
- (23) Kim, S. J.; Chung, T. H.; Bae, S. H. *Thin Solid Films* **2009**, *517*, 4251–4254.
- (24) Walsh, J. L.; Konga, M. G. *Appl. Phys. Lett.* **2008**, *93*, 111501–3.
- (25) Shibata, J.; Shimizu, K.; Satokawa, S.; Satsuma, A.; Hattori, T. *Phys. Chem. Chem. Phys.* **2003**, *5*, 2154–2160.
- (26) Richter, M.; Bentrup, U.; Eckelt, R.; Schneider, M.; Pohl, M.-M.; Fricke, R. *Appl. Catal., B* **2004**, *51*, 261–274.
- (27) Meunier, F. C.; Breen, J. P.; Zuzaniuk, V.; Ross, J. R. H. *J. Catal.* **1999**, *187*, 493–505.

- (28) Meunier, F. C.; Zuzaniuk, V.; Breen, J. P.; Olsson, M.; Ross, J. R. *H. Catal. Today* **2000**, *59*, 287–304.
- (29) Tamm, S.; Ingelsten, H. H.; Palmqvist, A. E. C. *J. Catal.* **2008**, *255*, 304–312.
- (30) Iglesias-Juez, A.; Hungría, A. B.; Martínez-Arias, A.; Fuente, A.; Fernández-García, M.; Anderson, J. A.; Conesa, J. C.; Soria, J. *J. Catal.* **2003**, *217*, 310–323.
- (31) Yu, Y.; He, H.; Feng, Q.; Gao, H.; Yang, X. *Appl. Catal., B* **2004**, *49*, 159–171.
- (32) Chansai, S.; Burch, R.; Hardacre, C.; Breen, J.; Meunier, F. *J. Catal.* **2010**, *276*, 49–55.
- (33) Chansai, S.; Burch, R.; Hardacre, C.; Breen, J.; Meunier, F. *J. Catal.* **2011**, *281*, 98–105.
- (34) Bion, N.; Saussey, J.; Hedouin, C.; Seguelong, T.; Daturi, M. *Phys. Chem. Chem. Phys.* **2001**, *3*, 4811–4816.
- (35) Bion, N.; Saussey, J.; Haneda, M.; Daturi, M. *J. Catal.* **2003**, *217*, 47–58.
- (36) Algwari, Q. Th. Plasma jet formation and interactions between atmospheric pressure dielectric barrier discharge. Ph.D. thesis, The Queen's University of Belfast, 2011.
- (37) Breen, J. P.; Burch, R.; Hardacre, C.; Hill, C. J.; Rioche, C. *J. Catal.* **2007**, *246*, 1–9.
- (38) Chansai, S.; Burch, R.; Hardacre, C.; Norton, D.; Bao, X.; Lewis, L. *Appl. Catal., B* **2014**, *160–161*, 356–364.
- (39) Burch, R.; Breen, J. P.; Meunier, F. C. *Appl. Catal. B* **2002**, *39*, 283–303.
- (40) Shimizu, K.; Satsuma, A.; Hattori, T. *Appl. Catal., B* **2000**, *25*, 239–247.
- (41) Eränen, K.; Klingstedt, F.; Arve, K.; Lindfors, L. E.; Murzin, D. *Y. J. Catal.* **2004**, *227*, 328–343.
- (42) Ji, Y.; Todd, J. T.; Crocker, M. *Appl. Catal. B* **2013**, *140–141*, 265–275.
- (43) Lee, D. H.; Lee, J.-O.; Kim, K.-T.; Song, Y.-H.; Kim, E.; Han, H.-K. *Int. J. Hydrogen Energy* **2012**, *37*, 3225–3233.
- (44) Ricard, A.; Nouvellon, C.; Konstantinidis, S.; Dauchot, J. P.; Wautelet, M.; Hecq, M. *J. Vac. Sci. Technol. A* **2002**, *20*, 1488–1491.